

The Search for $\eta(1440) \rightarrow K_S^0 K^\pm \pi^\mp$ in Two-Photon Fusion at CLEO

R. Ahohe,¹ D. M. Asner,¹ S. A. Dytman,¹ W. Love,¹ S. Mehrabyan,¹ J. A. Mueller,¹ V. Savinov,¹ Z. Li,² A. Lopez,² H. Mendez,² J. Ramirez,² G. S. Huang,³ D. H. Miller,³ V. Pavlunin,³ B. Sanghi,³ E. I. Shibata,³ I. P. J. Shipsey,³ G. S. Adams,⁴ M. Chasse,⁴ M. Cravey,⁴ J. P. Cummings,⁴ I. Danko,⁴ J. Napolitano,⁴ H. Muramatsu,⁵ C. S. Park,⁵ W. Park,⁵ J. B. Thayer,⁵ E. H. Thorndike,⁵ T. E. Coan,⁶ Y. S. Gao,⁶ F. Liu,⁶ R. Stroynowski,⁶ M. Artuso,⁷ C. Boulahouache,⁷ S. Blusk,⁷ J. Butt,⁷ E. Dambasuren,⁷ O. Dorjkhaidav,⁷ J. Li,⁷ N. Menaa,⁷ R. Mountain,⁷ R. Nandakumar,⁷ R. Redjimi,⁷ R. Sia,⁷ T. Skwarnicki,⁷ S. Stone,⁷ J. C. Wang,⁷ K. Zhang,⁷ S. E. Csorna,⁸ G. Bonvicini,⁹ D. Cinabro,⁹ M. Dubrovin,⁹ A. Bornheim,¹⁰ S. P. Pappas,¹⁰ A. J. Weinstein,¹⁰ R. A. Briere,¹¹ G. P. Chen,¹¹ T. Ferguson,¹¹ G. Tatishvili,¹¹ H. Vogel,¹¹ M. E. Watkins,¹¹ J. L. Rosner,¹² N. E. Adam,¹³ J. P. Alexander,¹³ K. Berkelman,¹³ D. G. Cassel,¹³ V. Crede,¹³ J. E. Duboscq,¹³ K. M. Ecklund,¹³ R. Ehrlich,¹³ L. Fields,¹³ R. S. Galik,¹³ L. Gibbons,¹³ B. Gittelman,¹³ R. Gray,¹³ S. W. Gray,¹³ D. L. Hartill,¹³ B. K. Heltsley,¹³ D. Hertz,¹³ L. Hsu,¹³ C. D. Jones,¹³ J. Kandaswamy,¹³ D. L. Kreinick,¹³ V. E. Kuznetsov,¹³ H. Mahlke-Krüger,¹³ T. O. Meyer,¹³ P. U. E. Onyisi,¹³ J. R. Patterson,¹³ D. Peterson,¹³ J. Pivarski,¹³ D. Riley,¹³ A. Ryd,¹³ A. J. Sadoff,¹³ H. Schvarthoff,¹³ M. R. Shepherd,¹³ S. Stroiney,¹³ W. M. Sun,¹³ J. G. Thayer,¹³ D. Urner,¹³ T. Wilksen,¹³ M. Weinberger,¹³ S. B. Athar,¹⁴ P. Avery,¹⁴ L. Breva-Newell,¹⁴ R. Patel,¹⁴ V. Potlia,¹⁴ H. Stoeck,¹⁴ J. Yelton,¹⁴ P. Rubin,¹⁵ C. Cawlfield,¹⁶ B. I. Eisenstein,¹⁶ G. D. Gollin,¹⁶ I. Karliner,¹⁶ D. Kim,¹⁶ N. Lowrey,¹⁶ P. Naik,¹⁶ C. Sedlack,¹⁶ M. Selen,¹⁶ J. Williams,¹⁶ J. Wiss,¹⁶ K. W. Edwards,¹⁷ D. Besson,¹⁸ T. K. Pedlar,¹⁹ D. Cronin-Hennessy,²⁰ K. Y. Gao,²⁰ D. T. Gong,²⁰ Y. Kubota,²⁰ T. Klein,²⁰ B. W. Lang,²⁰ S. Z. Li,²⁰ R. Poling,²⁰ A. W. Scott,²⁰ A. Smith,²⁰ C. J. Stepaniak,²⁰ S. Dobbs,²¹ Z. Metreveli,²¹ K. K. Seth,²¹ A. Tomaradze,²¹ P. Zweber,²¹ J. Ernst,²² A. H. Mahmood,²² K. Arms,²³ K. K. Gan,²³ and H. Severini²⁴

(CLEO Collaboration)

¹University of Pittsburgh, Pittsburgh, Pennsylvania 15260

²University of Puerto Rico, Mayaguez, Puerto Rico 00681

³Purdue University, West Lafayette, Indiana 47907

⁴Rensselaer Polytechnic Institute, Troy, New York 12180

⁵University of Rochester, Rochester, New York 14627

⁶Southern Methodist University, Dallas, Texas 75275

⁷Syracuse University, Syracuse, New York 13244

⁸Vanderbilt University, Nashville, Tennessee 37235

⁹Wayne State University, Detroit, Michigan 48202

¹⁰California Institute of Technology, Pasadena, California 91125

¹¹Carnegie Mellon University, Pittsburgh, Pennsylvania 15213

¹²Enrico Fermi Institute, University of Chicago, Chicago, Illinois 60637

¹³Cornell University, Ithaca, New York 14853

¹⁴University of Florida, Gainesville, Florida 32611

¹⁵George Mason University, Fairfax, Virginia 22030

¹⁶University of Illinois, Urbana-Champaign, Illinois 61801

¹⁷Carleton University, Ottawa, Ontario, Canada K1S 5B6
and the Institute of Particle Physics, Canada

¹⁸*University of Kansas, Lawrence, Kansas 66045*

¹⁹*Luther College, Decorah, Iowa 52101*

²⁰*University of Minnesota, Minneapolis, Minnesota 55455*

²¹*Northwestern University, Evanston, Illinois 60208*

²²*State University of New York at Albany, Albany, New York 12222*

²³*Ohio State University, Columbus, Ohio 43210*

²⁴*University of Oklahoma, Norman, Oklahoma 73019*

(Dated: January 10, 2005)

Abstract

We analyze 13.8 fb^{-1} of the integrated e^+e^- luminosity collected at 10.6 GeV center-of-mass energy with the CLEO II and CLEO II.V detectors to study exclusive two-photon production of hadrons with masses below 1.7 GeV/c^2 decaying into the $K_S^0 K^\pm \pi^\mp$ final state. We observe two statistically significant enhancements in the $\eta(1440)$ mass region. These enhancements have large transverse momentum which rules them out as being due to pseudoscalar resonances but is consistent with the production of axial-vector mesons. We use tagged two-photon events to study the properties of the observed enhancements and associate them with the production of $f_1(1285)$ and $f_1(1420)$. Our non-observation of $\eta(1440)$ is inconsistent by more than two standard deviations with the first observation of this resonance in two-photon collisions by the L3 experiment. We present our estimates for 90% confidence level upper limits on the products of two-photon partial widths of pseudoscalar hadrons and their branching fractions into $K_S^0(\pi^+\pi^-)K^\pm\pi^\mp$.

I. INTRODUCTION

A key to understanding the phenomenon of quark and gluon confinement in Quantum Chromodynamics (QCD) is the experimental observation and analysis of the properties of various hadronic bound states predicted by the quark model, Lattice QCD (LQCD), Flux Tube and other theories[1, 2]. One of the main emphases in hadronic physics has long been on the discovery of exotic hadronic resonances and “extranumerals” which could not be explained within the framework of the quark model. For example, the Flux Tube model and LQCD (even when the quenching approximation is lifted) predict a large number of light glueballs – bound states of the carriers of strong interaction – and of hybrids – hadrons composed of three constituents, two quarks and a gluon. A large number of potential candidates for such new states of hadronic matter have been discovered over the past 35 years in many experiments[3]. In our opinion, most of these candidates need to be confirmed and remain to be understood. One such candidate is the $\eta(1440)$ resonance first observed in 1967 in $p\bar{p}$ annihilation at rest into $K\bar{K}\pi\pi^+\pi^-$. This resonance has also been seen in radiative decays of J/ψ into $K\bar{K}\pi$ and in charge-exchange hadronic reaction $\pi^-p \rightarrow \eta\pi\pi n$. Until recently, the $\eta(1440)$ had been seen only in gluon-rich environments, and this established it as a prominent glueball candidate. Alternatively, $\eta(1440)$ and another mysterious pseudoscalar hadron, $\eta(1295)$, might be radial excitations of the η and η' mesons.

One way to discriminate among the ground state meson, radial excitation, and glueball hypotheses is to measure a hadron’s two-photon partial width, $\Gamma_{\gamma\gamma}$. Assuming that quantum numbers allow a two-photon decay, $\Gamma_{\gamma\gamma}$ would be of the order keV for a ground state meson, approximately an order of magnitude smaller for a radial excitation[4], and of a vanishingly small value for a true glueball, because photons couple to gluons only through an intermediate quark loop. A two-photon partial width is usually measured using inverse two-photon decay, *i.e.*, in the process of single hadron production in e^+e^- scattering, where the hadron is born in the fusion of two space-like photons emitted by the beam electron and the positron. It is also possible that light glueballs and pseudoscalar mesons, such as the $\eta(1440)$, are mixed, and their parameters, including $\Gamma_{\gamma\gamma}$, should be obtained from global fits to the light hadron spectrum. In 2001 a new piece was added to the $\eta(1440)$ puzzle, when the L3 experiment reported[5] the first observation of the $\eta(1440)$ in two-photon collisions. L3 measured $\eta(1440)$ ’s two-photon partial width to be 212 ± 50 (stat.) ± 23 (sys.) eV, assuming it decays only to $K\bar{K}\pi$. The other poorly understood hadron decaying to $K\bar{K}\pi$, $\eta(1295)$, has still not been observed in two-photon collisions.

In this paper we seek corroborating evidence for the L3’s observation of the $\eta(1440)$. Using a data sample that exceeds that of L3 by a factor of five, we do not observe this resonance. In our analysis, we study the reaction $e^+e^- \rightarrow e^+e^-\mathcal{R}$, where the hadron \mathcal{R} (of mass below 1.7 GeV/c²) is produced by two space-like photons, decays to $K\bar{K}\pi$, and is reconstructed in its decay to the final state $K_S^0 K^\pm \pi^\mp$.¹ The secondary vertex associated with the decay $K_S^0 \rightarrow \pi^+\pi^-$ helps to identify $K\bar{K}\pi$ production. The presence of four charged final state particles helps to trigger on such events. The quantity that allows us to distinguish between two-photon and other production processes for pseudoscalar mesons is the transverse momentum p_\perp , which is the component of the hadronic system’s total vector momentum perpendicular to the beam axis. The properties of the e^+e^- scattering amplitude demand two-photon events peak sharply at small p_\perp , except when a single axial-

¹ Charge-conjugated states are implied throughout this paper.

vector meson, such as $f_1(1285)$, $f_1(1420)$, or $f_1(1510)$ is produced. The production of these mesons in inverse two-photon decay is suppressed by the Landau-Yang theorem[6] for real photons. Therefore, the production cross sections for axial-vector mesons are enhanced at intermediate p_\perp . Finally, most of the time, the scattered electron and positron carry a large fraction of the event energy away in the direction of the beam and are not detected, *i.e.*, remain “untagged”. When the scattered electron or positron is detected (“tagged”) in the calorimeter, the tag and the hadronic system are recoiling against each other and, most of the time, their momenta are collinear in the plane perpendicular to the beam axis.

In our analysis, we study the $K_S^0 K^\pm \pi^\mp$ final state in two regimes: in the untagged mode with p_\perp below 0.6 GeV/c and in the tagged mode where p_\perp usually exceeds 1.0 GeV/c. Taking into account the integrated e^+e^- luminosities and two-photon production cross sections for pseudoscalars, our event sample in the $\eta(1440)$ mass region exceeds that of the L3 experiment by a factor of five. We reported preliminary results of our analysis in the untagged mode previously[7].

This paper is organized as follows: first, we briefly describe our detector, data sample, and our two-photon Monte Carlo generators. Then, we present the analysis procedure and the calibration data sample. The section on our results for the pseudoscalar production and systematic errors is followed by the section describing the analysis of axial-vector mesons and the conclusions. The main result of our study is the non-observation of the $\eta(1440)$ in our data sample where we expected 114 ± 28 such events according to the results published by the L3 experiment[5].

II. EXPERIMENTAL APPARATUS AND DATA SAMPLE

The results presented here are obtained from data corresponding to an integrated e^+e^- luminosity of 13.8 fb^{-1} . The data were collected at the energies of the $\Upsilon(4S)$ resonance mass and 60 MeV below it at the Cornell Electron Storage Ring (CESR) with the CLEO detector. The first third of the data was recorded with the CLEO II configuration of the detector[8], which consisted of three cylindrical drift chambers placed in an axial solenoidal magnetic field of 1.5T, a CsI(Tl)-crystal electromagnetic calorimeter, a time-of-flight (TOF) plastic scintillator system and a muon system (proportional counters and copper strips embedded at various depths in steel absorbers). Two thirds of the data were taken with the CLEO II.V configuration of the detector where the innermost drift chamber was replaced by a silicon vertex detector[9] (SVX) and the argon-ethane gas of the main drift chamber was changed to a helium-propane mixture. This upgrade led to improved resolutions in momentum and, to lesser extent, in specific ionization energy loss (dE/dx) measurements.

When the data were collected, the information from the two outer drift chambers, the TOF system, and electromagnetic calorimeter was used to make the decisions in the three-tier CLEO trigger system[10] complemented by a software filter for beam-gas event rejection. The response of the detector is modeled with a Monte Carlo (MC) program based on the GEANT 3 simulation framework[11]. The data and simulated samples are processed by the same event reconstruction program. Whenever possible, the efficiencies are either calibrated or corrected for the difference between simulated and actual detector responses using direct measurements from independent data samples.

III. MONTE CARLO GENERATORS FOR TWO-PHOTON EVENTS

To lowest order in perturbation theory, the amplitude for hadron production in the process of two-photon fusion can be factorized into two terms. The first term describes the emission of space-like photons by the electron and the positron and is completely calculable in QED. The second term deals with the production of a single C -even hadron by these photons. This, essentially *hadronic* part of the amplitude depends on the structure of a particular hadronic resonance and can be parametrized in terms of its two-photon partial width and transition form factors. To describe the factorization of the amplitude and to relate a production cross section to the two-photon partial width of a hadron, we employ a theoretical framework developed independently by several theorists and conveniently summarized by V.M. Budnev *et al.*[12]. In this framework, the QED part of the amplitude is calculated using helicity tensors for fluxes of incoming photons of various polarizations. The hadronic part of the amplitude is described by transition form factors which are the functions of Q^2 , *i.e.* the masses of the space-like photons. In our previous analysis[14], we demonstrated that light pseudoscalar mesons have similar transition form factors that can be parametrized in terms of pole-mass parameters. Helicity and parity conservation laws and Bose symmetry imply that only transverse photons interact to produce pseudoscalar final states. This holds even for highly space-like photons and explains why there is only one transition form factor that affects the cross section for $e^+e^- \rightarrow e^+e^-\eta(1440)$. We choose the pole-mass parameter that determines Q^2 evolution of this transition form factor to be a commonly used value of 770 MeV (which is *coincidentally* close to the ρ meson mass). However, our results for pseudoscalar mesons are insensitive to the value of this parameter. This is the case because most of the cross section for pseudoscalar production comes from the low Q^2 region, where transition form factors are unimportant. We show the generator-level distribution of p_\perp for the $\eta(1440)$ signal MC in Fig. 1. There is a strong correlation between Q^2 and p_\perp^2 in case of pseudoscalar production but only at very small p_\perp^2 . The momentum transfer Q^2 cannot be reconstructed unambiguously for untagged events, so we use p_\perp (which is measured using the hadronic system alone) in our analysis. Note that for the axial-vector mesons, Q^2 can be reconstructed with excellent accuracy from the measurements for the tagging electron without using the hadronic system.

Two Monte Carlo generators were developed at CLEO for two-photon studies. Both generators are based on the same theoretical framework[12] and extensively employ an importance sampling technique to simulate the divergent QED part of the two-photon amplitudes. Our two Monte Carlo generators for pseudoscalar production differ mainly by their user interfaces. Numerical predictions made using these programs are practically identical, *e.g.*, both generators predict the η_c production cross section at 10.58 GeV to be 2.4 pb per 1.0 keV two-photon partial width. The generator we use for the analysis described in this paper parametrizes wide resonances by relativistic Breit-Wigners for two-body decays. For narrow resonances, the difference between the cross sections evaluated using narrow-width approximation and this more realistic treatment of the running mass is approximately 1%. Both generators predict angular distributions of the decay products correctly and were employed in all previously published CLEO publications on two-photon production[13]. We emphasize our high confidence in the quality of our MC generators, because their numerical predictions are very important for measuring two-photon partial widths and transition form factors.

Assuming that transition form factors are known, the two-photon partial width $\Gamma_{\gamma\gamma}(\mathcal{R})$

of the resonance \mathcal{R} can be measured (up to the uncertainty in branching fractions) from data

$$\Gamma_{\gamma\gamma}(\mathcal{R}) \mathcal{B}(K_S^0(\pi^+\pi^-)K^\pm\pi^\mp) \text{ (keV)} = \frac{N^{\text{data}}}{\mathcal{L} \epsilon \sigma^{\text{MC}}} \quad (1)$$

where N^{data} is the estimate of the number of detected signal events, \mathcal{L} is the integrated e^+e^- luminosity of the data sample, ϵ is the overall trigger and reconstruction efficiency (excluding branching fractions), and σ^{MC} is the numerically predicted cross section for the process $e^+e^- \rightarrow e^+e^-\mathcal{R}$ with $\Gamma_{\gamma\gamma}(\mathcal{R}) = 1 \text{ keV}$. We evaluate the cross sections σ^{MC} numerically using our MC generators. These quantities depend on the assumptions about the transition form factors, the electron beam energy, the mass and full width of the resonance \mathcal{R} , and on the beam polarization, although the CESR beams are not polarized.

Axial-vector mesons have zero two-photon partial width, and some additional model input is necessary to approximate their transition form factors. For our analysis, we implement the model of Cahn[15] where axial-vector mesons are treated as non-relativistic $q\bar{q}$ states. In this model, the production cross section is determined by the normalization parameter $\tilde{\Gamma}_{\gamma\gamma}$ and by the transition form factors driven by a single pole-mass parameter. In this model, even if $\tilde{\Gamma}_{\gamma\gamma}$ is fixed, the pole-mass parameter has a strong impact on the production rate. This explains the dramatic difference in the magnitudes of cross sections for axial-vector mesons shown in Fig. 1 for pole-mass parameters of 400 MeV and 770 MeV. This feature of Cahn's model for axial-vector production cross sections was previously noticed by the TPC/2 γ experiment[16] when they estimated the strength of the $f_1(1420)$ coupling to space-like photons, $\mathcal{B}_{K\bar{K}\pi}\tilde{\Gamma}_{\gamma\gamma} = 1.3 \pm 0.5 \pm 0.3 \text{ keV}$, by assuming a pole-mass of 770 MeV. The parameter $\tilde{\Gamma}_{\gamma\gamma}$ provides an overall normalization in Cahn's model, while the differential cross section approaches zero, as it should, in the limit $p_\perp^2 \rightarrow 0$.

IV. ANALYSIS PROCEDURE

In our untagged analysis, we select events with exactly four charged tracks that are reconstructed in the region of the detector where trigger and detection efficiencies are well understood and associated systematic errors are under control. We require at least one charged track with transverse momentum exceeding 250 MeV/c. The projection of this track is required to point to the barrel part of the calorimeter (*i.e.* with $|\cos\theta| \leq 0.71$, where the polar angle, θ , is measured with respect to the beam direction). We only use events recorded with trigger configurations designed to be efficient for events with at least two charged hadrons in the final state. The latter three requirements select events recorded with a well-understood trigger. This is an important step in our analysis, because most untagged two-photon pseudoscalar events cannot be triggered on. The overall efficiency of these criteria is 9%. The efficiency of our trigger (including a software filter developed to reject cosmic, beam-gas and beam-wall events) for the $\eta(1440)$ signal is only 43%. Note that, in a fashion typical for two-photon studies, we quote the trigger efficiency for events that satisfy kinematic selection. This simplifies the evaluation of uncertainties in the trigger and reconstruction efficiencies. While the trigger efficiency is small, our confidence in knowing its relative uncertainty (14%) is high. This confidence is based on dedicated trigger efficiency measurements performed for this purpose at CLEO[14, 17, 18].

Furthermore, we need to suppress backgrounds arising from non-signal two-photon events, τ pairs and one-photon e^+e^- annihilation to hadrons, the first two being the most important

contributions. To suppress such background events, it is useful to identify the presence of hadrons with s quarks, since many of the background events do not contain them. Remaining events often come from τ pairs or two-photon events with extra particles (charged or neutral) besides the four reconstructed charged hadrons associated with the possible signal. Background events where a substantial amount of energy is carried away by the undetected particles usually have large missing transverse momentum (*e.g.* in case of neutrinos). In background events we often detect photons in the calorimeter (especially in case of τ pairs). Non-signal two-photon events with some low-momentum particles escaping detection could also pose a problem, unless we require p_\perp to be small.

To suppress these backgrounds, we identify K_S^0 candidates by reconstructing secondary vertices radially displaced by at least two standard deviations (σ) from the primary interaction point. The secondary vertex is required to satisfy a set of criteria developed to reduce systematic uncertainty in the K_S^0 reconstruction efficiency. The reconstructed mass of the K_S^0 candidate is required to be within $\pm 5\sigma$ from its nominal value. The $K_S^0 K^\pm \pi^\mp$ signal-event candidates are required to have only one such K_S^0 . The remaining two charged tracks are identified using dE/dx and TOF information. The measurements of dE/dx and TOF for these tracks in signal-event candidates with $K_S^0 K^\pm \pi^\mp$ masses below 1.7 GeV/c² are shown in Fig. 2. These measurements are used to form a reduced- χ^2 under the different particle identification (PID) hypotheses, normalized by the number of available measurements. We require the square root of the reduced- χ^2 to be less than three. There is negligible PID ambiguity associated with this selection for the $\eta(1440)$ candidates in CLEO. PID requirements are not imposed on the daughter pions from K_S^0 candidates in the $K_S^0 K^\pm \pi^\mp$ analysis. The efficiency of K_S^0 and PID selection is approximately 50%. The unmatched neutral energy, defined to be the total amount of energy collected in photon-like calorimeter clusters that do not match the projections of charged tracks, is required to be below 100 MeV (though one cluster of 1 GeV or more is allowed for tagged events, as discussed in more detail later). This requirement is powerful in rejecting background from τ pairs. Calorimeter clusters with small amounts of energy could often be present in signal events because of “split-off” effects caused by nuclear interactions of charged hadrons with the materials of the detector. The unmatched neutral energy requirement is 65% efficient. Some of the quoted efficiencies depend on the assumptions about the mass, full width and the decay dynamics of the $\eta(1440)$. We study these dependencies in our analysis. This is discussed later.

In our analysis, p_\perp is the most important quantity that discriminates between pseudoscalars born from untagged two-photon fusion and other production mechanisms. The core part of the p_\perp resolution function is well described by a Gaussian shape with $\sigma = 7$ MeV. However, approximately 15% of signal MC events show a p_\perp bias towards larger reconstructed values, and the tail stretches to 100 MeV/c. We show the difference between the reconstructed and generated scalar values of p_\perp , the p_\perp resolution function, in Fig. 3 for the $\eta(1440)$ signal MC after applying all but the p_\perp selection criteria. The curve shows the result of a Gaussian fit to the core part of the distribution which contains 85% of the area. To suppress combinatorial background, untagged events are required to have p_\perp below 100 MeV/c. The efficiency of this selection is 65%. Many of the events rejected by this selection are of two-photon origin, where some of the final state particles are not reconstructed. An example of such feed-down would be the two-photon production of final states $K^* \bar{K}^* n(\pi)$ (where $n \geq 0$ is the number of pions). Cross sections for these processes have never been measured. The $p_\perp \leq 100$ MeV/c requirement strongly suppresses such backgrounds without compromising the efficiency for signal events. We show the distribution of the $K_S^0 K^\pm \pi^\mp$

invariant mass for untagged events in Fig. 4(a) after all selection criteria are applied. The invariant mass distribution for K_S^0 candidates (after kinematically constraining K_S^0 daughters to come from a common secondary vertex) from these events is shown in Fig. 5. We discuss our interpretation of Fig. 4(a) in Section VI.

In the tagged event sample, in addition to identifying a $K_S^0 K^\pm \pi^\mp$ candidate, we require the presence of a calorimeter cluster with energy of at least 1 GeV and not matching the projections of four signal charged tracks into the calorimeter. We assume that this cluster is produced by the tagging electron or positron which radiated the highly off-shell photon in the two-photon process. If we find a high-momentum charged track matched to this energy cluster, we assume that it is produced by the tag. Two-photon tagging is possible on CLEO for polar angles larger than 12° . However, at such small angles, the tags barely scrape the endcap calorimeter, and tagging efficiency is small. For scattering angles between 15° and 20° , at least 25% of the tag energy is usually detected (typically, the tagging electron carries at least 4 GeV/c momentum). For larger scattering angles, the showers are almost fully contained, and the entire energy of the tag is detectable. For scattering angles above 22.5° , calorimeter information is complemented by the track reconstruction and independent measurement of the tag's momentum. For angles above 25° , the trigger efficiency approaches 100%. A more detailed description of tag identification can be found in our previous publication[14]. No transverse momentum requirement is imposed on tagged two-photon events.

To suppress misreconstructed hadronic background, we require the tag and the $K_S^0 K^\pm \pi^\mp$ candidate to be collinear within five degrees in the (r, ϕ) plane perpendicular to the beam axis. The distribution of the collinearity angle, which is the deviation of the tag's direction from being opposite to that of hadronic system, for signal event candidates in data is shown in Fig. 6. This figure also shows the fit to the data with a signal line shape from MC simulation for axial-vector two-photon production and a linear approximation to the background contribution. The shape of the collinearity distribution is determined by the QED part of the amplitude and by resolution: while most of the time the undetected electron (or positron) transfers some energy to the hadronic system, it continues to travel in the direction of the beam. This explains the signal shape for the collinearity shown in Fig. 6. The distribution of $K_S^0 K^\pm \pi^\mp$ invariant mass for tagged events is shown in Fig. 4(d). We discuss our interpretation of the invariant mass enhancements observed in this figure in Section VII.

V. CALIBRATION DATA SAMPLE

The particular values of the selection criteria used in our analysis are optimized to provide the best discrimination between the signal and background and/or to reduce systematic uncertainties in the final results. In these optimizations, the expected number of the $\eta(1440)$ signal events is estimated from the L3 measurement, and the background level is estimated from data without inspecting the $\eta(1440)$ signal mass region.

To measure the efficiencies of our selection criteria and to evaluate systematic errors, we use a calibration data sample where we find exactly two high-quality K_S^0 candidates. To establish the two-photon origin for these events, daughter pions from the K_S^0 pairs are required to have a PID-based reduced- $\chi^2 \leq 9$. The reconstructed masses of the K_S^0 candidates are required to be between 491 GeV/c² and 505 GeV/c². We use the distributions of these events' transverse momentum and unmatched neutral energy to analyze their consistency with the two-photon production mechanism. After applying the described selection criteria,

the $K_S^0 K_S^0$ purity of the calibration data sample is found to be at least 98%, *i.e.* most selected events are due to exclusive two-photon production of K_S^0 pairs. We show the $K_S^0 K_S^0$ invariant mass for data events selected in this procedure in Fig. 7. To study the efficiencies in the range of momenta for final state hadrons from $K_S^0 K^\pm \pi^\mp$ signal, only $K_S^0 K_S^0$ events with invariant mass below 1.4 GeV/c² (*i.e.* events to the left of the vertical line in Fig. 7) are used to evaluate the efficiencies and to estimate systematic uncertainties for the $K_S^0 K^\pm \pi^\mp$ analysis. The transverse momentum distributions for our calibration K_S^0 pairs in data and MC are shown in Fig. 8. In this figure, to demonstrate that non two-photon contribution is small, the $K_S^0 K_S^0$ MC sample is normalized to the data at transverse momentum values below 100 MeV/c. The comparison between MC and calibration data indicates no background contribution at a statistically noticeable level. To study the efficiencies of our selection criteria, we loosen and apply them individually to the $K_S^0 K_S^0$ data and MC samples. In each study, we estimate the $K_S^0 K_S^0$ purity of the calibration data sample using the shape of p_\perp for K_S^0 pairs. We do not find any statistically significant deviations between MC efficiencies and their estimates obtained from our calibration data sample. The statistics of the latter sample are used to estimate systematic uncertainties of our selection criteria.

VI. UPPER LIMITS FOR PSEUDOSCALAR PRODUCTION

In our analysis, we study the final state $K_S^0 K^\pm \pi^\mp$ in two distinct kinematic regions: untagged and tagged. We use untagged events with $p_\perp \leq 100$ MeV/c to obtain the results for pseudoscalar mesons. Tagged events are used to shed light on the untagged high- p_\perp sample. We observe no production of the $\eta(1440)$ or any other resonance in Fig. 4(a) and conclude that the two-photon production of $\eta(1440)$ is below our sensitivity. The points with the error bars in this figure show our data, and the solid curve is the result of a binned maximum likelihood (ML) fit described below. The dashed curves show the expected $\eta(1440)$ signal and its $\pm 1 \sigma$ (statistical) deviations according to L3, superimposed on the results of our fit.

To estimate the upper limit on the number of signal events, we assume that there is only one resonance potentially decaying into $K_S^0 K^\pm \pi^\mp$ in the mass region between 1.3 GeV/c² and 1.7 GeV/c². We perform a binned ML fit to the distribution shown in Fig. 4(a) with the signal line shape for the $\eta(1440)$ and a third order polynomial approximating the background contribution. There are several steps involved in estimating the signal line shape from MC: first, we convolute a two-body relativistic Breit-Wigner for a pseudoscalar meson with the two-photon luminosity function. Then, we correct the resulting function with the detector resolution and efficiency functions. Using the mass and full width of the $\eta(1440)$ obtained by the L3 experiment, $M = 1481 \pm 12$ MeV/c² and $\Gamma = 48 \pm 9$ MeV, we expect 114 ± 28 signal events in our data. From the results of our ML fit, we estimate the upper limit on the number of $\eta(1440)$ signal events to be less than 48 at 90% Confidence Level (CL), which is 2.4σ (stat.) below the prediction based on the L3 observation.

To estimate the upper limit on the two-photon partial width of the $\eta(1440)$, we divide our 90% CL upper limit on the number of signal events by the product of the overall detection efficiency (0.76%) reduced by one unit of systematic uncertainty (30%), the integrated e^+e^- luminosity (13.8 fb⁻¹) and our numerical prediction for the pseudoscalar two-photon cross section (33 pb/keV) (see Eq. 1). The efficiency quoted above assumes the L3 mass and full width for the $\eta(1440)$ and its phase-space decay to $K\bar{K}\pi$. The high inefficiency arises primarily from the kinematics of two-photon collisions. Combining all these numbers, we

obtain a Bayesian upper limit of $\Gamma_{\gamma\gamma}(1440)\mathcal{B}(K_S^0(\pi^+\pi^-)K^\pm\pi^\mp) < 20.4$ eV (at 90% CL), which is to be compared to the L3 value of 49 ± 12 (stat.) eV (with 11% systematic error). We repeat these estimates for various hypotheses for $M(1440)$ and $\Gamma(1440)$ and show our results in Fig. 9.

It is possible that the $\eta(1440)$ predominantly decays into \bar{K}^*K followed by the decay $K_S^0K^\pm\pi^\mp$. We study this scenario by imposing an additional selection criterion on the $K_S^0\pi^\mp$ or $K^\pm\pi^\mp$ invariant mass, requiring at least one combination to be within the K^* mass window 0.84–0.94 GeV/c². After applying this requirement, we repeat the analysis described above and arrive at the 90% CL upper limits shown in Fig. 10. To make the estimates shown in this figure, we properly account for the K^* polarization because it affects the reconstruction efficiency.

In addition to the lack of an $\eta(1440)$ signal, we do not observe any events in the $\eta(1295)$ mass region and use the upper limit of 2.3 signal events (at 90% CL) to estimate the production rate. This translates into an upper limit of $\Gamma_{\gamma\gamma}(1295)\mathcal{B}(K\bar{K}\pi) < 14$ eV at 90% CL using the mass and full width obtained by the previous experiments[3]. To convert our results into upper limits on $\Gamma_{\gamma\gamma}\mathcal{B}(K\bar{K}\pi)$ we use $\mathcal{B}(K_S^0 \rightarrow \pi^+\pi^-) = 0.686$ and $\mathcal{B}(K\bar{K}\pi \rightarrow K_S^0K^\pm\pi^\mp) = 1/3$.

We test our analysis technique by estimating the two-photon partial width of the η_c that we reported recently in an independent analysis of the same data sample[19]. That analysis measures $\Gamma_{\gamma\gamma}(\eta_c) = 7.5 \pm 0.5$ (stat.) ± 0.5 (sys.) keV, while our estimate is $\Gamma_{\gamma\gamma}(\eta_c) = 7.0 \pm 0.7$ (stat.) keV. Our estimates, performed independently with the CLEO II and CLEO II.V data samples are 7.1 ± 1.3 (stat.) keV and 7.0 ± 0.9 (stat.) keV, respectively. Our larger statistical error is due to the restrictive nature of our unmatched neutral energy and transverse momentum criteria.

The dominant sources of systematic error in the overall efficiency are the uncertainties in the four-track event selection (21%), trigger efficiency (14%), the unmatched neutral energy requirement (10%), and the transverse momentum (10%) requirement, all of which are added in quadrature. The 21% uncertainty in four-track selection consists of two 15% uncertainties. The first 15% error reflects the uncertainty in the detector simulation of efficiency loss for charged tracks at small polar angles (with respect to the beam direction). We evaluate this error by comparing the measurements of efficiency loss in our calibration data sample and in signal MC as a function of polar angles for the final state charged particles. The data and MC agreed, but we decide to use the statistical uncertainty on the comparison as our systematic error, which is 15%. The other 15% uncertainty is due to requiring exactly four charged tracks reconstructed in event candidates. To estimate the uncertainty associated with this selection criterion, we allow more than four charged tracks in our calibration data sample and in signal MC. Then we measure the efficiency of four charged tracks selection criterion. Again, the two samples agree on the efficiency, but we take the statistical uncertainty of the comparison, which is dominated by the data statistics. The uncertainty in the trigger efficiency is primarily due to imperfect knowledge of its value for events with a small number of charged hadrons. To estimate this uncertainty, we measure the trigger efficiencies in data using partially independent trigger condition configurations. These efficiencies are implemented in our detector simulation on a particle-by-particle basis. However, the deficiencies of our GEANT 3-based MC program in simulating hadronic interactions of charged hadrons in the calorimeter result in a 14% uncertainty in the trigger efficiency for four-track events. The uncertainties in the unmatched neutral energy and transverse momentum selection criteria are determined by the statistics of our calibration data sample. For these

two criteria, there is also a good agreement between the data and our two-photon MC for low-mass K_S^0 pairs.

Our upper limits for $\eta(1440)$ production are inconsistent with the first observation of this resonance by the L3 experiment at a level of greater than 2σ . To estimate our upper limits, we have to make some assumptions about the invariant mass shape for background contribution. We do not take into account the effect of possible interference between resonant and continuum two-photon production of $K_S^0 K^\pm \pi^\mp$.

VII. AXIAL-VECTOR MESONS $f_1(1285)$ AND $f_1(1420)$

After observing no pseudoscalar signals at low p_\perp , we inspect the distributions of $K_S^0 K^\pm \pi^\mp$ invariant mass in untagged events at larger p_\perp . These distributions are shown in Figs. 4(b) and (c). At intermediate p_\perp , shown in Fig. 4(b), we see no indication of $\eta(1295)$ and $\eta(1440)$ which is consistent with our non-observation of these hadrons at lower transverse momentum. However, Fig. 4(c) indicates two enhancements for $K_S^0 K^\pm \pi^\mp$ events with $200 \text{ MeV/c} < p_\perp < 600 \text{ MeV/c}$. Fitting this untagged high- p_\perp mass distribution to the $\eta(1295)$ (using the nominal mass and width[3]), and to the $\eta(1440)$ (using L3's mass and width) on top of a third order polynomial for the combinatorial background², we find 214 ± 33 events in the higher mass enhancement and 48 ± 13 events in the lower mass enhancement. We investigate the hypothesis that our observations are due to statistical fluctuations of untagged $\eta(1440)$ signal events, which should populate the low- p_\perp region, into the high- p_\perp region between 200 MeV/c and 600 MeV/c . We perform 10,000 toy MC experiments to estimate the probability for 200 pseudoscalar two-photon events to fluctuate to this p_\perp region in the presence of the background observed in data. In each toy MC experiment, we use the shape of the invariant mass distribution for background and the number of background events estimated from data in the high p_\perp region. In every run we also generate 200 signal toy MC events with the predicted p_\perp distribution. These signal toy MC events are then merged with the toy background sample. Then, we perform a binned ML fit to the mass distribution for the high p_\perp region and estimate the central value for the number of signal $\eta(1440)$ events. All our toy MC experiments yield less than 120 $\eta(1440)$ events, with a peak in the distribution of signal yield at 55 ± 16 events. Therefore, we estimate the signal fluctuation probability to be less than 10^{-4} . This is not surprising because transverse momentum distributions for two-photon MC (shown in Fig. 1) and calibration two-photon data (shown in Fig. 8) peak sharply towards small values.

We use previous measurements from TPC/2 γ [16] and our Monte Carlo generator for two-photon axial-vector production to estimate the expected rate for the $f_1(1420)$ signal in the high- p_\perp region (between 200 MeV/c and 600 MeV/c) to be 200 ± 50 events, which is consistent with the observed 214 ± 33 events. Also, the enhancement at lower invariant mass in data, shown in Fig. 4(c), is consistent with the $f_1(1285)$ hypothesis. These two mesons, $f_1(1285)$ and $f_1(1420)$, are the only axial-vectors consistent with quark model predictions. However, because our untagged events contain at least one missing particle, it is impossible to rule out backgrounds from some other processes, such as hadronic decays of τ leptons

² For the fit shown in Fig. 4(c), we use the masses and the widths we obtain from our fit to the tagged mass distribution shown in Fig. 4(d).

or threshold enhancements in two-photon production of $K^* \bar{K}^* n(\pi)$.³ Therefore, we cannot claim the observation of two-photon production of axial-vector mesons solely on the basis of the untagged invariant mass distribution shown in Fig. 4(c).

To unambiguously establish the presence of axial-vector mesons in our data, we use the distribution of the invariant mass for tagged two-photon events shown in Fig. 4(d). The statistics shown in this figure allow us to perform ML fits for the masses and the widths of both enhancements. Our results are $M = 1284 \pm 3 \text{ MeV}/c^2$ and $\Gamma = 25 \pm 6 \text{ MeV}$ for the lower mass enhancement, and $M = 1441 \pm 3 \text{ MeV}/c^2$ and $\Gamma = 67 \pm 9 \text{ MeV}$ for the higher mass enhancement. This is consistent with the results of previous experiments[3] for the $f_1(1285)$ and $f_1(1420)$. From our fits, we conclude that both invariant mass enhancements in Figs. 4(c) and (d) are due to axial-vector two-photon production. The $f_1(1420)$ assignment is supported by the strong signal for K^* decays observed in the Dalitz plot for the $f_1(1420)$ signal region in tagged data events, shown in Fig. 11(a). According to previous experiments[3], the $f_1(1420)$ indeed decays dominantly into the $\bar{K}^* K$ channel. The projections of the Dalitz plot are shown in Figs. 11(b) and (c), the $K_S^0 K^\pm \pi^\mp$ invariant mass distribution for the $f_1(1420)$ signal region is shown in Fig. 11(d). To be included in the latter distribution, at least one $K\pi$ combination is required to be in the K^* signal region indicated by the vertical and horizontal bands in Figs. 11(a),(b) and (c). In our fits, we approximate the resonances by two-body relativistic Breit-Wigners ignoring (small) resolution effects.

Our previous two-photon publication[14] demonstrated that, with CLEO, we can measure the invariant masses of light mesons with better than a few MeV accuracy. It is interesting to note that the enhancement we associate with the $f_1(1420)$ has its mass shifted relative to the nominal value of $1426.3 \pm 0.9 \text{ MeV}/c^2$ by more than four standard deviations while the width is consistent with $54.9 \pm 2.6 \text{ MeV}$ [3]. This discrepancy could be due to the interference with non-resonant two-photon continuum production that we do not take into account in our analysis. There is less non-resonant background in the $f_1(1285)$ mass region, and our estimates are indeed in a better agreement with the nominal values[3] of $M = 1281.8 \pm 0.6 \text{ MeV}/c^2$ and $\Gamma = 24.1 \pm 1.1 \text{ MeV}$. Our $K_S^0 K^\pm \pi^\mp$ invariant mass distributions show no indication of the $f_1(1510)$.

VIII. CONCLUSIONS

With a data sample that exceeds the L3 statistics by a factor of five, we cannot confirm their first observation of the $\eta(1440)$ in two-photon collisions. We report the upper limits $\Gamma_{\gamma\gamma}(1440)\mathcal{B}(K\bar{K}\pi) < 89 \text{ eV}$ (with the mass $1481 \text{ MeV}/c^2$ and full width 48 MeV according to L3 estimates[5]) and $\Gamma_{\gamma\gamma}(1295)\mathcal{B}(K\bar{K}\pi) < 14 \text{ eV}$ (assuming nominal mass and full width[3]) at 90% CL. The former number should be compared with the result reported by the L3 experiment $\Gamma_{\gamma\gamma}(1440)\mathcal{B}(K\bar{K}\pi) = 212 \pm 50 \text{ (stat.)} \pm 23 \text{ (sys.)}$. Our results for the $\eta(1440)$ are more than two standard deviations inconsistent with L3's measurements. Our upper limits on the two-photon partial widths of the $\eta(1295)$ and $\eta(1440)$ are consistent with the glueball and the radial excitation hypotheses.

We do not observe any pseudoscalar mesons with masses below $1.7 \text{ GeV}/c^2$ of sizable $\Gamma_{\gamma\gamma}$ decaying dominantly to $K\bar{K}\pi$. We observe only two ground-state axial-vector mesons

³ These backgrounds also complicate the analysis of two-photon resonances in the low- p_\perp region, but to a lesser degree than in untagged two-photon events of higher p_\perp .

in this mass region, consistent with quark model expectations. If the third axial-vector meson, the $f_1(1510)$, does exist, it may be a glueball or an exotic particle. In principle, it is possible that mesons and glueballs mix in nature. However, our observation of no extranumerical pseudoscalars and of exactly two axial-vector mesons decaying to $K\bar{K}\pi$ makes such an interesting but somewhat artificial scenario unnecessary to introduce for light hadrons decaying in this channel.

We expect to obtain definitive information on the existence and the origin of light pseudoscalar exotic hadrons decaying to $K\bar{K}\pi$ with our currently running CLEO-c experiment[20], where the analysis of radiative hadronic decays of ~ 1 billion J/ψ 's might result in the firm discovery of glueballs and light exotics. We gratefully acknowledge the effort of the CESR staff in providing us with excellent luminosity and running conditions. This work was supported by the National Science Foundation and the U.S. Department of Energy.

- [1] C.J. Morningstar and M. Peardon, *Phys. Rev.* **D60**, 034509 (1999).
- [2] C. Bernard *et. al.*, *Phys. Rev.* **D56**, 7039 (1997).
- [3] K. Hagiwara *et al.*, Review of Particle Properties, *Phys. Rev.* **D66**, 010001-493 (2002).
- [4] T. Barnes, N. Black and P.R. Page, *arXiv* <http://arXiv.org/abs/nucl-th/0208072>.
- [5] L3 Collab., M. Acciarri *et al.*, *Phys. Lett.* **B501**, 1 (2001).
- [6] L. F. Landau, *Dokl. Akad. Nauk. SSSR* **60**, 207 (1948); C. N. Yang, *Phys. Rev.* **77**, 242 (1950).
- [7] V. Savinov and R. Ahohe, CLEO Collaboration, *Nucl. Phys.* **A721**, 797c (2003), the Proceedings of the 16th International Conference on Particles and Nuclei, PANIC'02, Osaka, Japan, 30 September – 4 October, 2002, edited by H. Toki, K. Imai and T. Kishimoto, Elsevier (2003).
- [8] CLEO Collab., Y. Kubota *et al.*, *Nucl. Instrum. Methods* **A320**, 66 (1992).
- [9] T. Hill, *Nucl. Instrum. Methods* **A418**, 32 (1998).
- [10] CLEO Collab., C. Bebek *et al.*, *Nucl. Instrum. Methods* **A302**, 261 (1992).
- [11] R. Brun *et al.*, GEANT 3.15, CERN Report No. DD/EE/84-1 (1987).
- [12] M. Budnev *et al.*, *Phys. Rep.* **C15** (1975), 181.
- [13] For a list of all CLEO publications on two-photon processes up to 2001 see V. Savinov, CLEO Collaboration, eConf C010430 (2001) W03, SLAC Workshop on e^+e^- Physics at Intermediate Energies, <http://arXiv.org/abs/hep-ex/0106013>.
- [14] CLEO Collaboration, J. Gronberg *et al.*, *Phys. Rev.* **D57**, 33 (1998).
- [15] R.N. Cahn, *Phys. Rev.* **D35**, 3342 (1987); **D37**, 833 (1988).
- [16] TPC/2 γ Collaboration, H. Aihara *et al.*, *Phys. Rev.* **D38**, 1 (1988).
- [17] CLEO Collaboration, J. Dominick *et al.*, *Phys. Rev.* **D50**, 3027 (1994).
- [18] CLEO Collaboration, M. Artuso *et al.*, *Phys. Rev.* **D50**, 5484 (1994).
- [19] CLEO Collaboration, D. Asner *et al.*, *Phys. Rev. Lett.* **92**, 142001 (2004).
- [20] CLEO-c and CESR-s Working Group, CLNS 01/1742, <http://www.lepp.cornell.edu/public/CLEO/spoke/CLEOc/>.

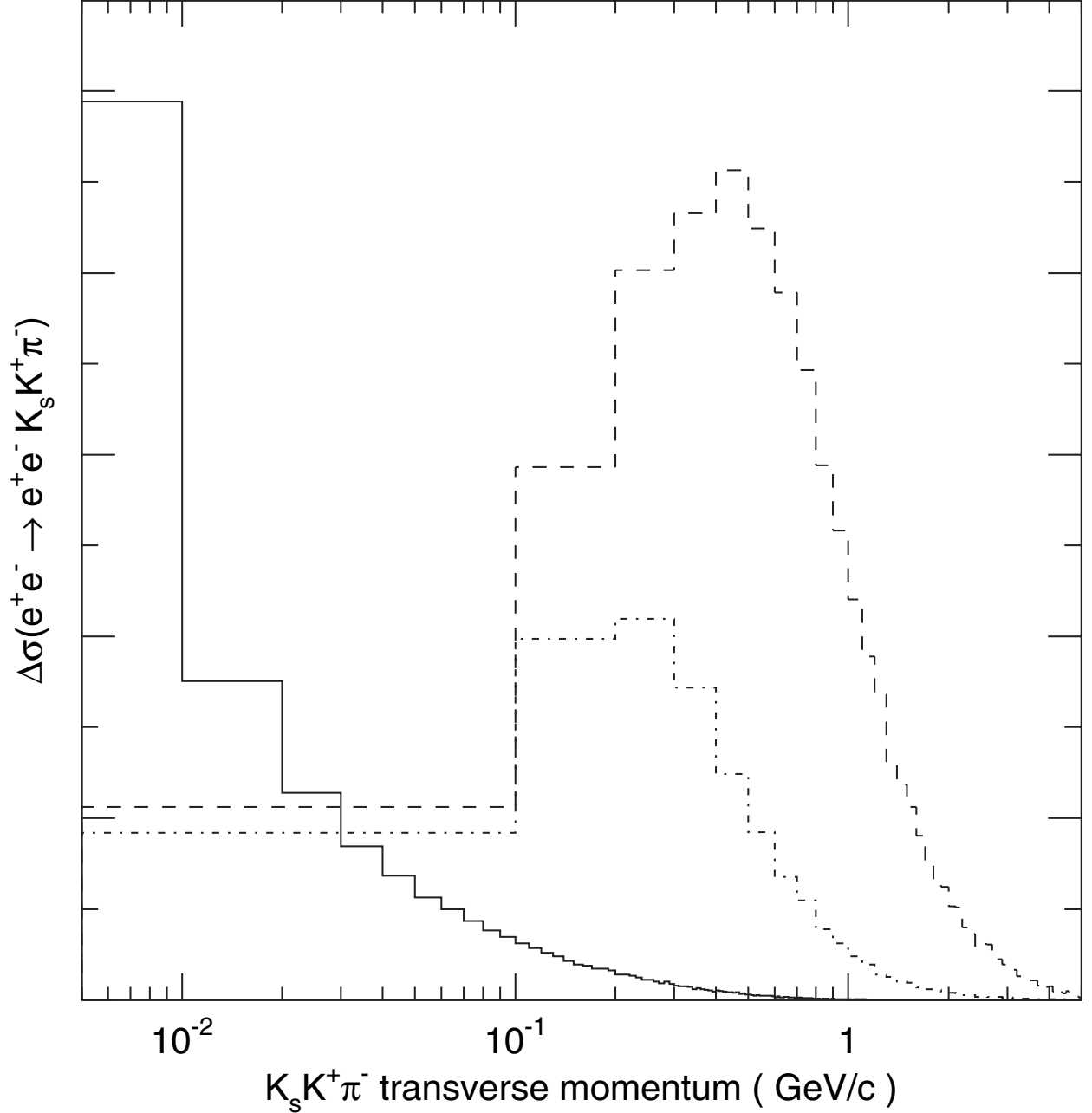


FIG. 1: The shapes of partial (*i.e.* integrated over p_\perp bins) cross sections $\Delta\sigma(e^+e^- \rightarrow e^+e^- \mathcal{R})$ for pseudoscalar (solid line, pole-mass parameter 770 MeV) and axial-vector (dashed and dashed-dotted lines for pole-mass parameters of 770 MeV and 400 MeV, respectively) mesons in MC at generator level. The distributions for axial-vector mesons are normalized to the same integrated luminosity. Note that a relatively small fraction of pseudoscalar events is expected in the region of P_\perp above 100 MeV/c , where most axial-vector mesons are produced.

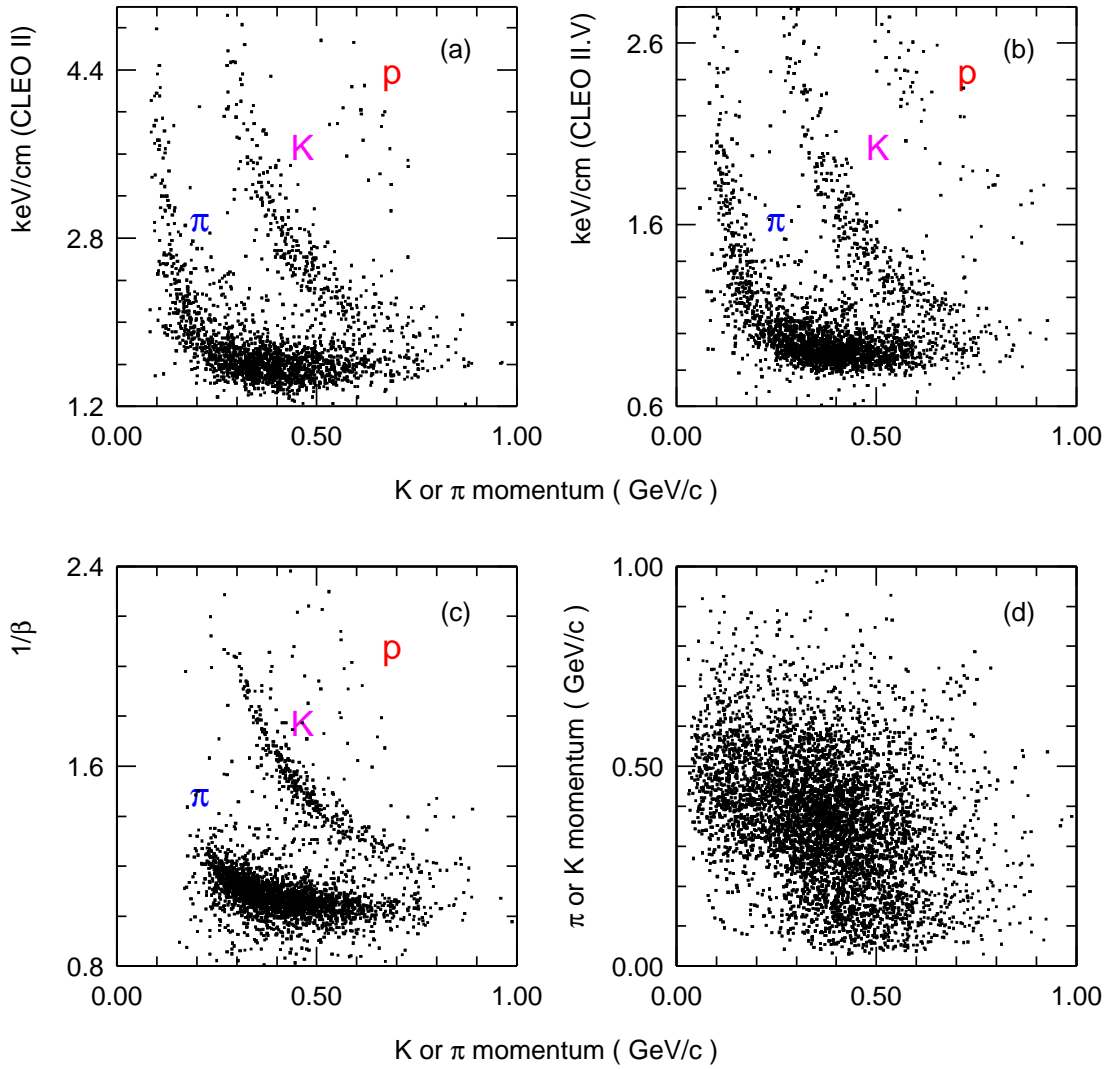


FIG. 2: The measurements of dE/dx for (a) CLEO II and (b) CLEO II.V, and (c) TOF versus charged track momentum (shown in (d) before applying the PID requirements) for untagged $K_S^0 K^\pm \pi^\mp$ data event candidates with invariant masses below $1.7 \text{ GeV}/c^2$ after all selection requirements but PID are applied.

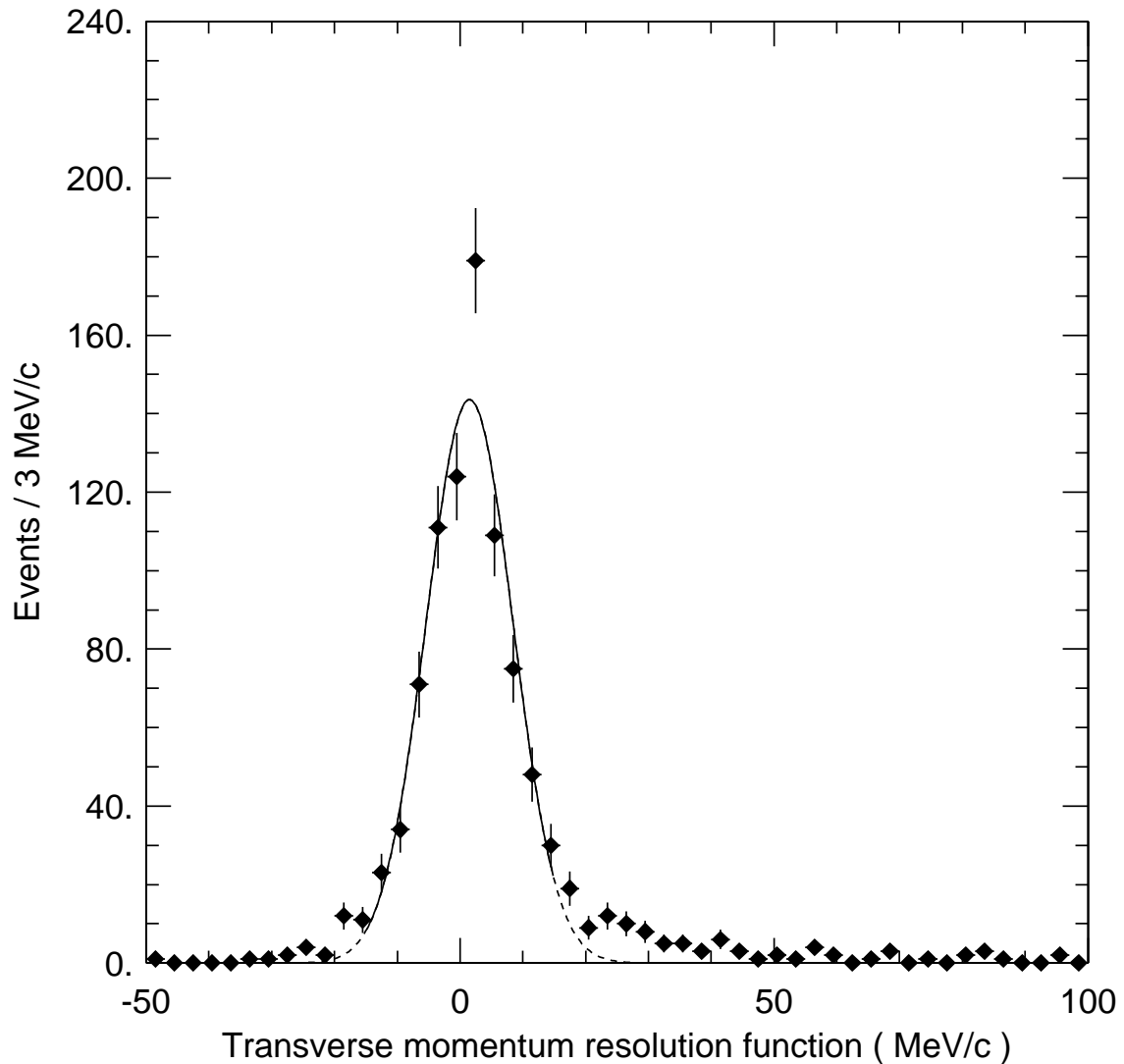


FIG. 3: The difference between the reconstructed and the generated scalar values of the p_{\perp} , for $\eta(1440) \rightarrow K_S^0 K^{\pm} \pi^{\mp}$ signal MC after all selection criteria but p_{\perp} are applied. The curve shows the result of a Gaussian fit to the core part of the distribution.

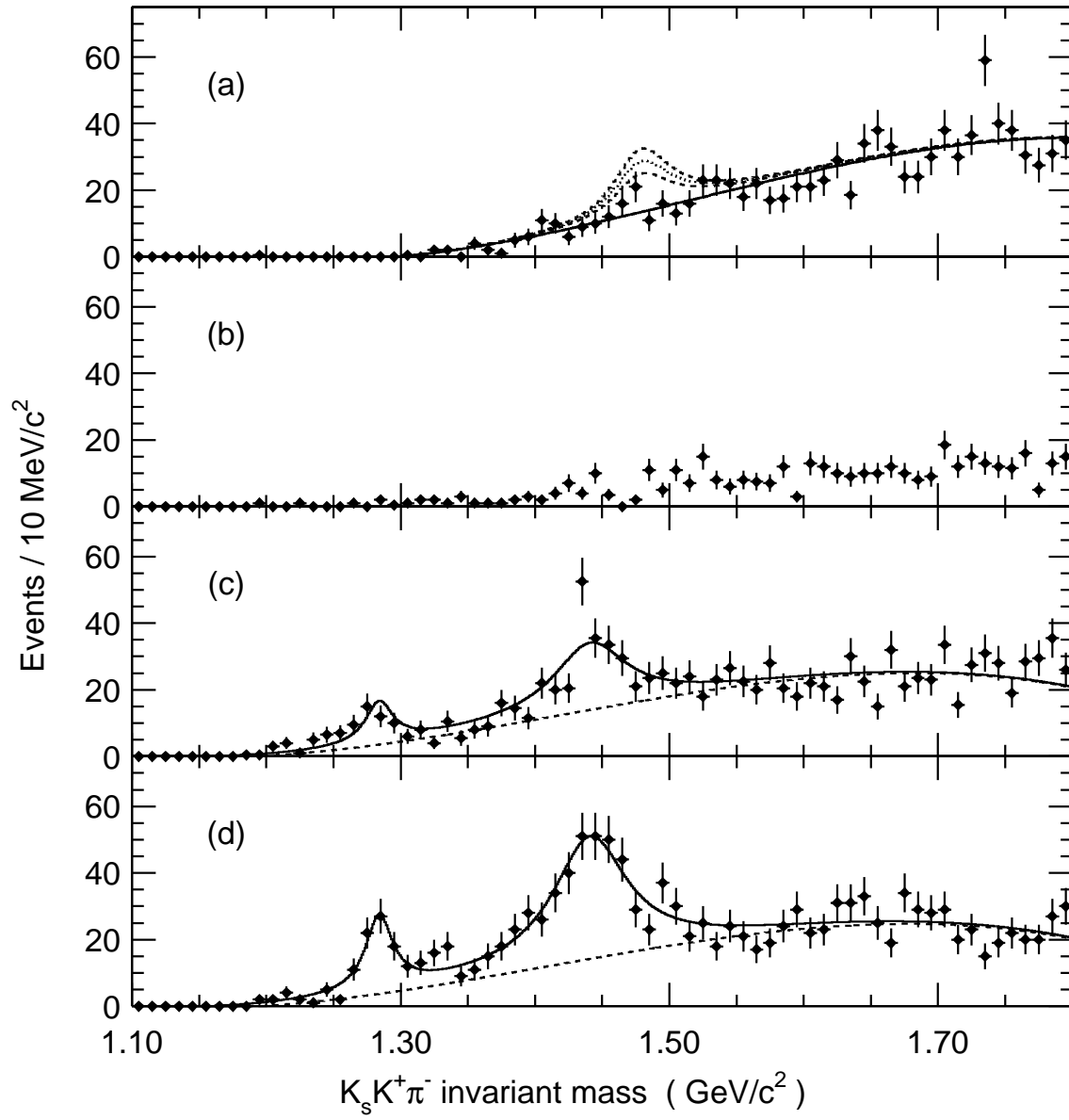


FIG. 4: The distributions of the $K_s^0 K^\pm \pi^\mp$ invariant mass for data events detected with (a) $p_\perp \leq 100$ MeV/c, (b) $100 \text{ MeV/c} \leq p_\perp \leq 200$ MeV/c and (c) $200 \text{ MeV/c} \leq p_\perp \leq 600$ MeV/c in the untagged mode, and (d) for all p_\perp in the tagged mode. The dashed curves in (a) show the strength of the expected $\eta(1440)$ signal according to the L3 results[5]. The solid curves in (a), (c) and (d) are the results of binned maximum likelihood fits for resonances with a polynomial approximation to the non-interfering combinatorial background. For (a), only the strength of the $\eta(1440)$ resonance is fit. For (c) and (d), the strength of $f_1(1285)$ and $f_1(1420)$ are fit. For the fit shown in (a), we use the mass and full width according to L3 estimates[5]. For the fit shown in (c), we use the masses and full widths obtained from our fit to the tagged invariant mass distribution shown in (d).

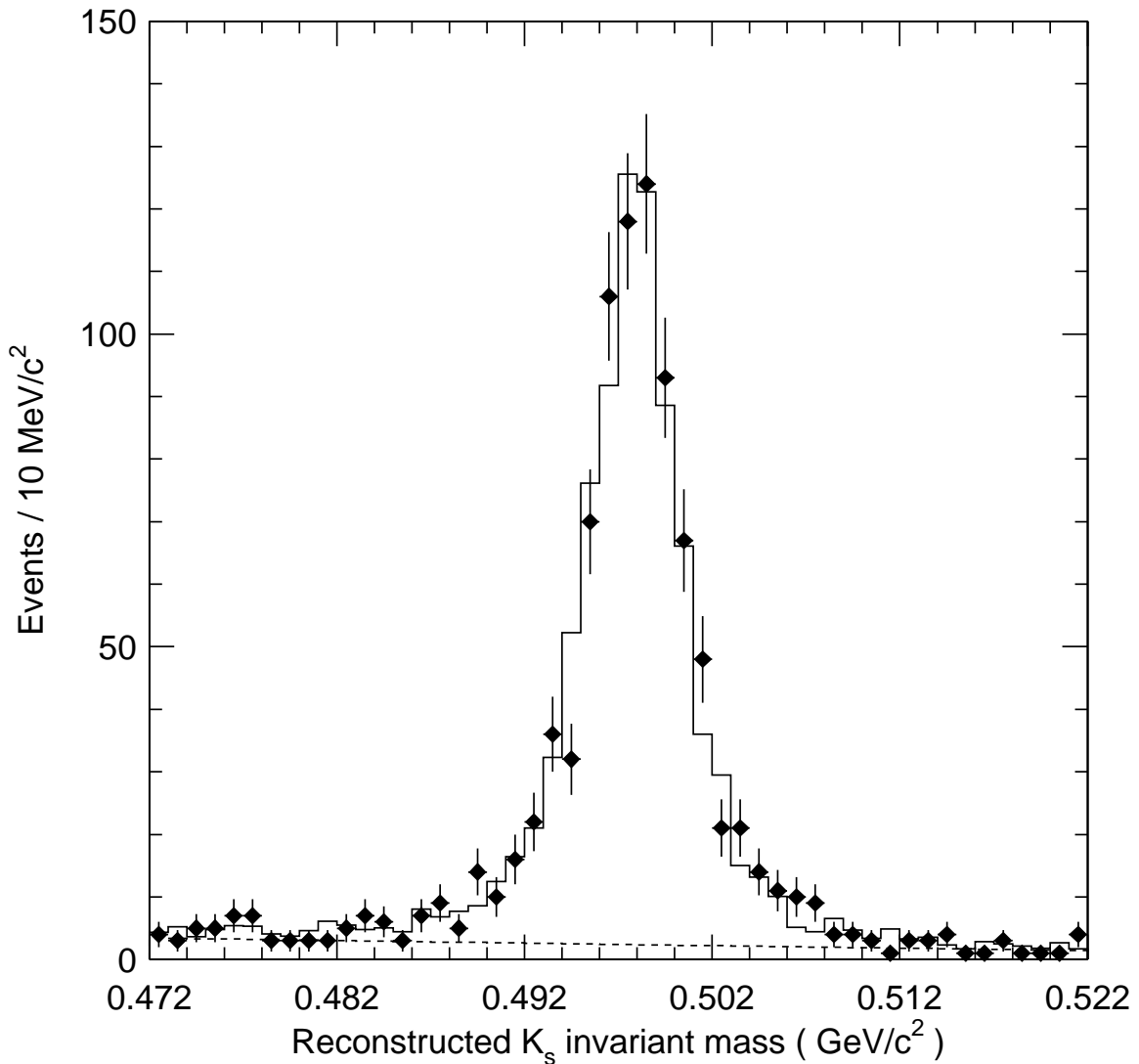


FIG. 5: Reconstructed invariant mass distribution for K_S^0 candidates from untagged $K_S^0 K^\pm \pi^\mp$ data event candidates with mass below $1.7 \text{ GeV}/c^2$ after all selection criteria are applied. Also shown is the result of the fit with K_S^0 MC shape and straight-line approximation to the combinatorial background.

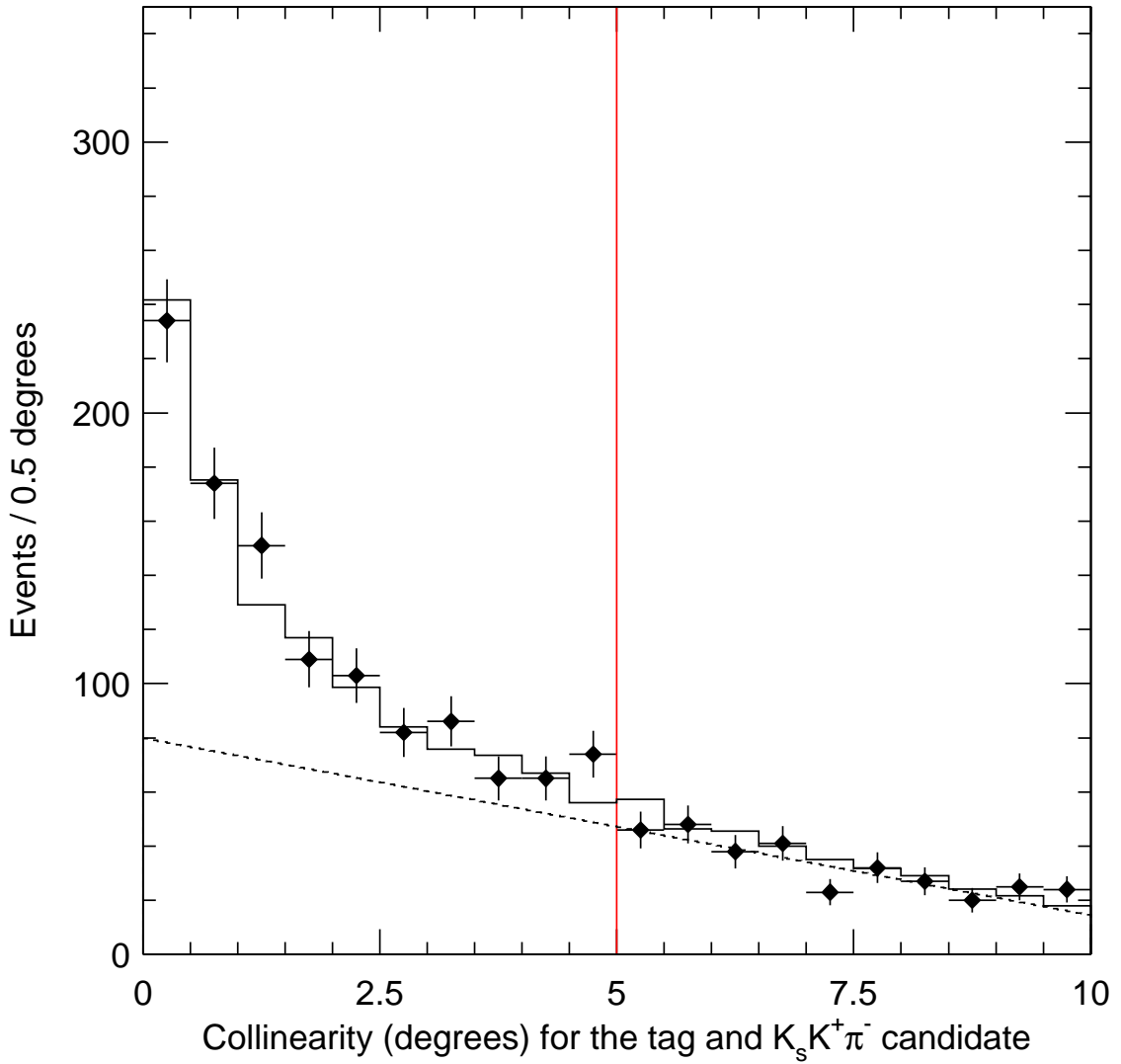


FIG. 6: The collinearity angle (degrees) between the $K_S^0 K^{\pm} \pi^{\mp}$ system and the tagging electron (or positron) in the plane perpendicular to the collision axis. The data are represented by the points with error bars. The dashed straight line approximates not-fully reconstructed two-photon events. The solid histogram is a fit to the data with the signal MC shape for axial-vector meson production and the aforementioned approximation for the background. The vertical line indicates the selection criterion for tagged events.

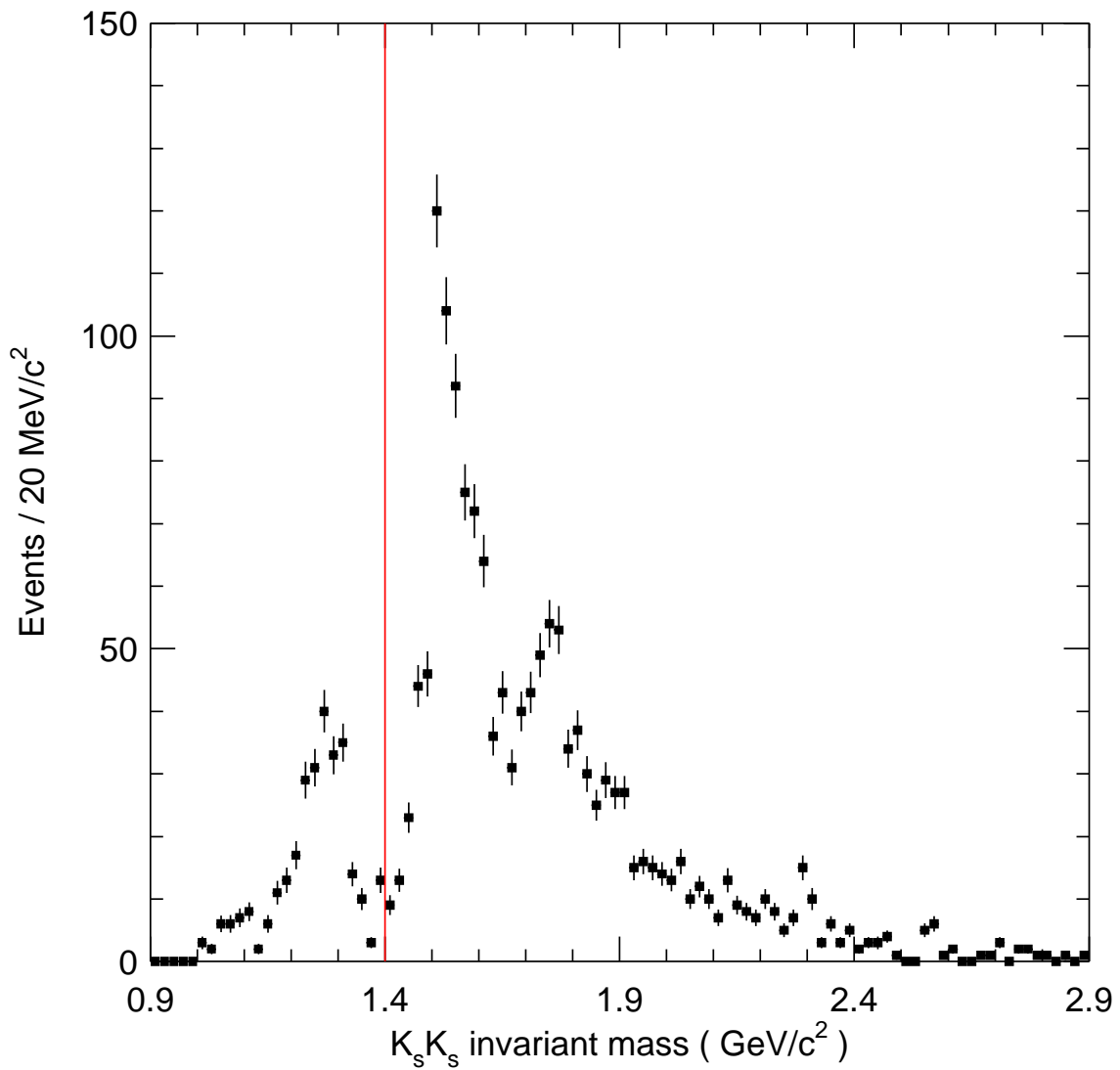


FIG. 7: The invariant mass of $K_S^0 K_S^0$ candidates in data. Events to the left of the vertical line are accepted for calibration and efficiency studies.

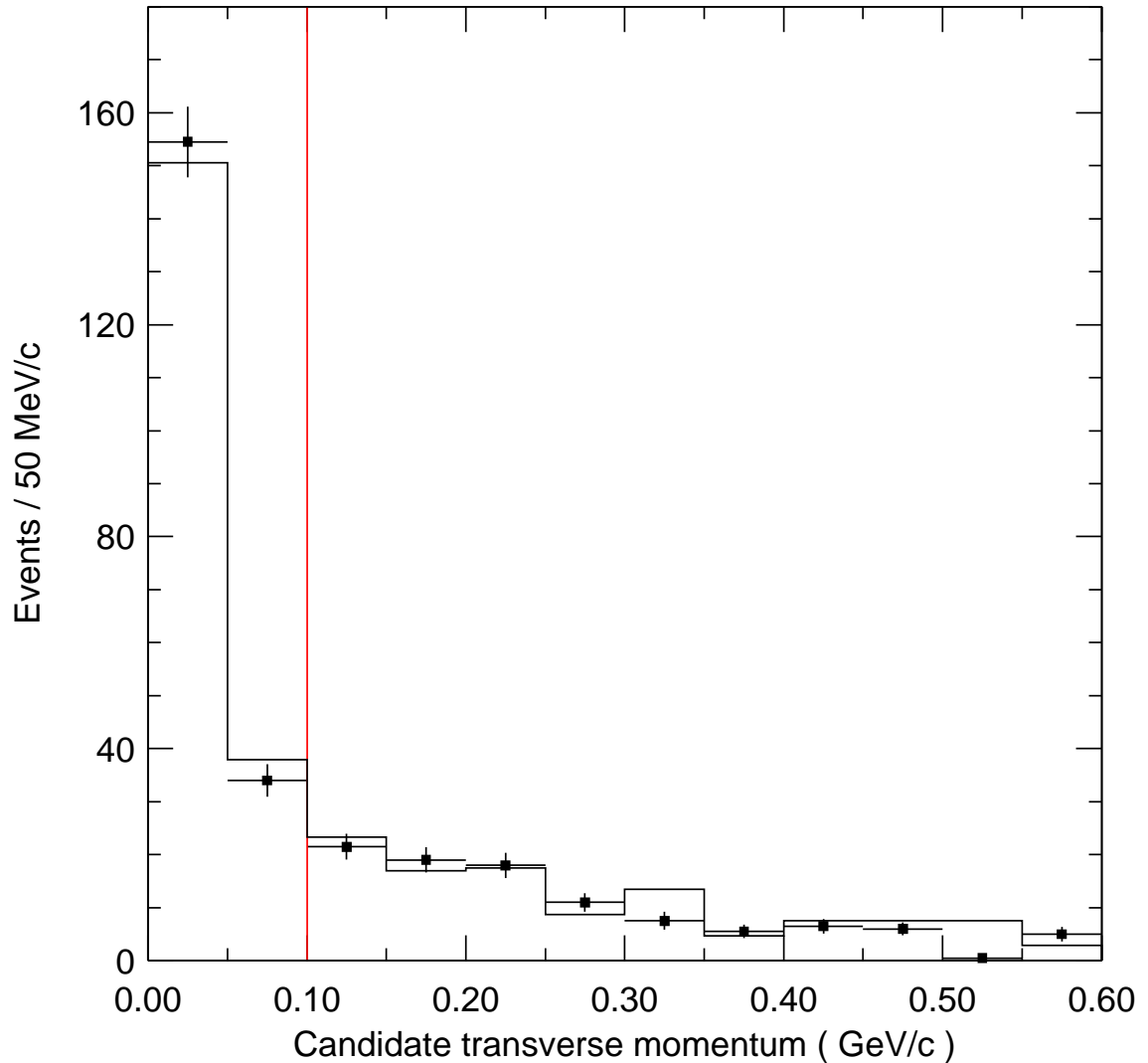


FIG. 8: Transverse momentum of $K_S^0 K_S^0$ candidates from the calibration data sample (points) and MC (solid histogram) after all selection criteria but p_\perp are applied. The MC distribution is normalized to data for p_\perp below 100 MeV/c, which is also the selection criterion applied to our $K_S^0 K^\pm \pi^\mp$ candidates in the untagged analysis.

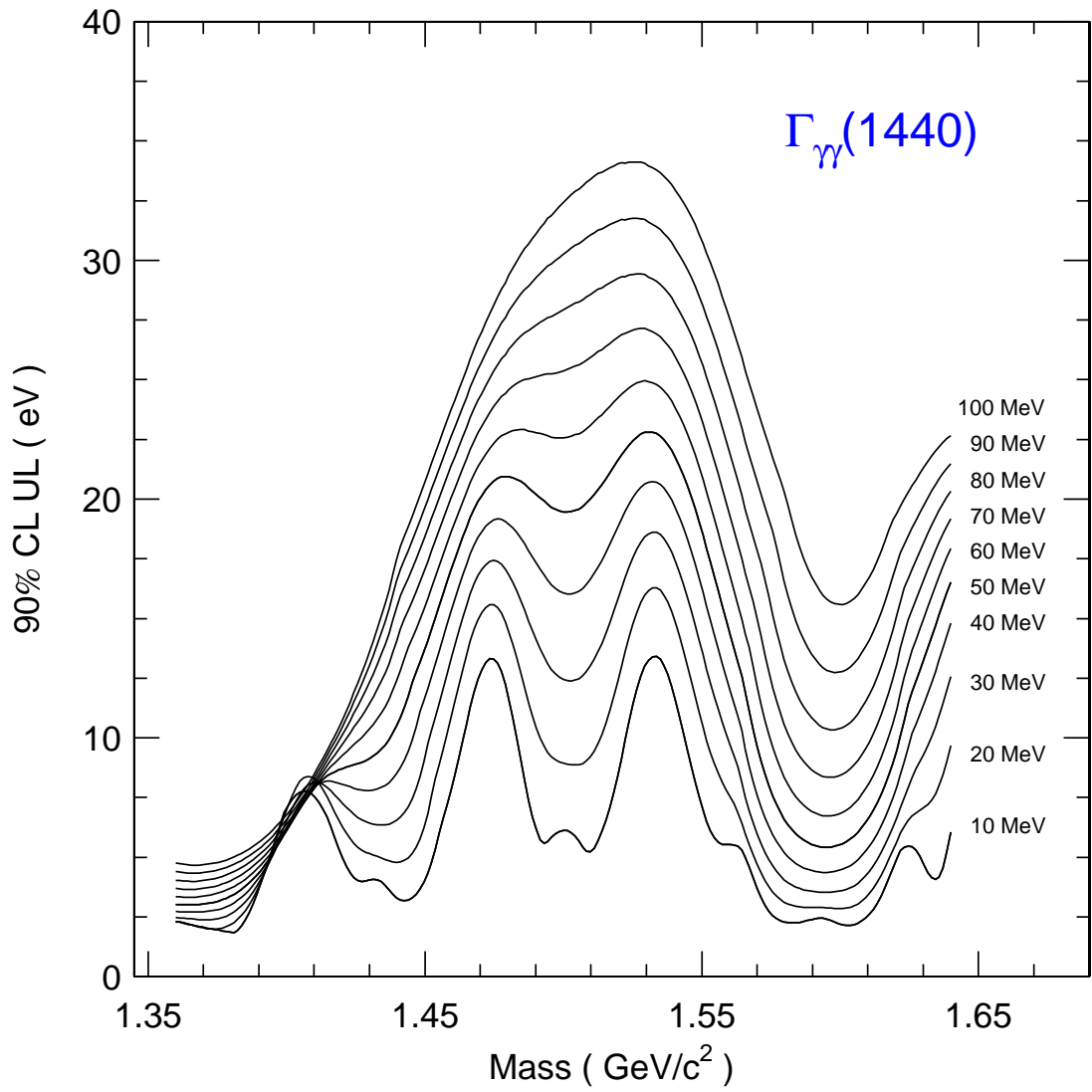


FIG. 9: 90% CL upper limits (in eV) on $\Gamma_{\gamma\gamma}(1440)\mathcal{B}(K_S^0(\pi^+\pi^-)K^\pm\pi^\mp)$ versus the mass of $\eta(1440)$ for various hypotheses for its full width assuming three body phase-space decay to $K_S^0K^\pm\pi^\mp$.

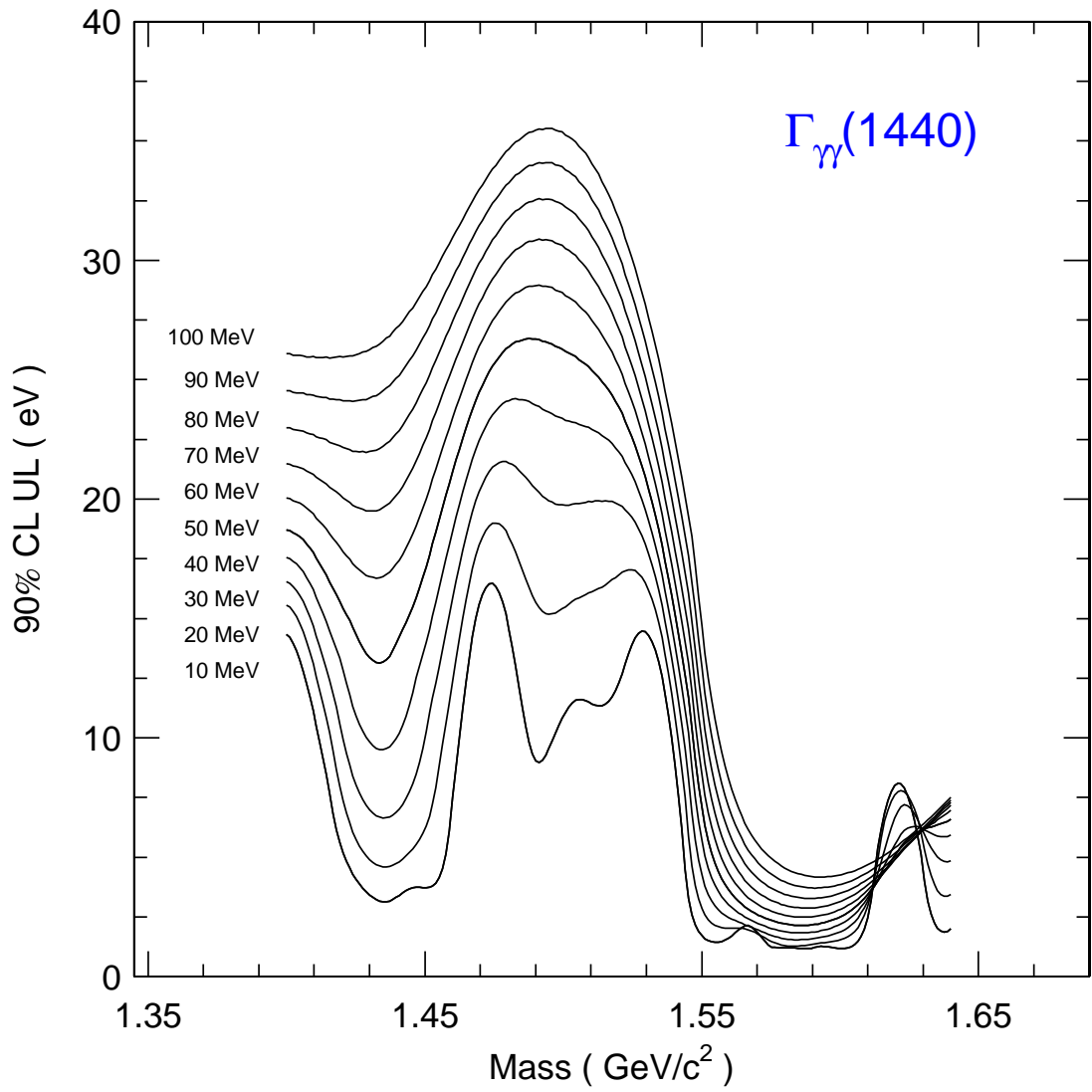


FIG. 10: 90% CL upper limits (in eV) on $\Gamma_{\gamma\gamma}(1440)\mathcal{B}(K_S^0(\pi^+\pi^-)K^\pm\pi^\mp)$ versus the mass of $\eta(1440)$ for various hypotheses for its full width assuming two body decay to \bar{K}^*K followed by the decay $K_S^0K^\pm\pi^\mp$.

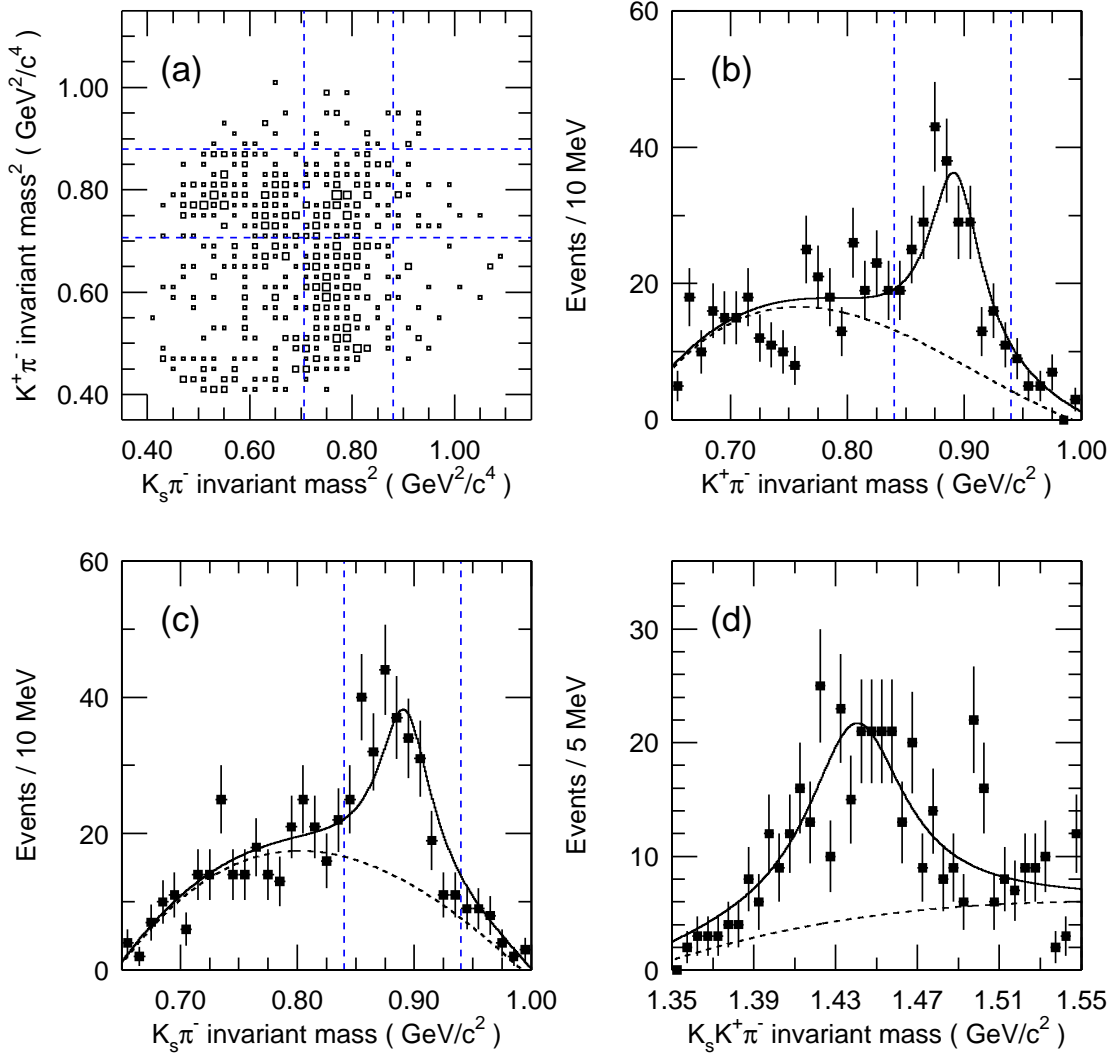


FIG. 11: Dalitz plot for $f_1(1420)$ candidates detected in tagged data events in the $K_S^0 K^\pm \pi^\mp$ invariant mass region between $1.35 \text{ GeV}/c^2$ and $1.55 \text{ GeV}/c^2$ (a). The projections of Dalitz plot on the $K^\pm \pi^\mp$ (b) and $K_S^0 \pi^\mp$ (c) invariant masses. The $K_S^0 K^\pm \pi^\mp$ invariant mass distribution (d) for data events with at least one $K\pi$ combination in the K^* mass region indicated by the vertical and horizontal bands in (a), (b) and (c). Solid and dashed curves show the results of the fits.